Dissecting p53 tumor suppressor functions in vivo

Clemens A. Schmitt,[1,4] Jordan S. Fridman,[1] Meng Yang,[2] Eugene Baranov,[2] Robert M. Hoffman,[2] and Scott W. Lowe[1,3]

[1]Cold Spring Harbor Laboratory, 1 Bungtown Road, Cold Spring Harbor, New York 11724
[2]AntiCancer Inc., 7917 Ostrow Street, San Diego, California 92111
[3]Correspondence: lowe@cshl.edu
[4]Present address: Max-Delbrück-Center for Molecular Medicine and Charité/Campus Virchow-Hospital, Department of Hematology/Oncology, Humboldt University, 13353 Berlin, Germany

Summary

Although the p53 tumor suppressor acts in a plethora of processes that influence cellular proliferation and survival, it remains unclear which p53 functions are essential for tumor suppression and, as a consequence, are selected against during tumor development. Using a mouse model harboring primary, genetically modified *myc*-driven lymphomas, we show that disruption of apoptosis downstream of p53 by Bcl2 or a dominant-negative caspase 9 confers—like p53 loss—a selective advantage, and completely alleviates pressure to inactivate p53 during lymphomagenesis. Despite their *p53*-null-like aggressive phenotype, apoptosis-defective lymphomas that retain intact *p53* genes do not display the checkpoint defects and gross aneuploidy that are characteristic of *p53* mutant tumors. Therefore, apoptosis is the only p53 function selected against during lymphoma development, whereas defective cell-cycle checkpoints and aneuploidy are mere byproducts of p53 loss.

Introduction

The p53 tumor suppressor was initially identified as the "guardian of the genome" based on its ability to mediate a G1 arrest following DNA damage (Kastan et al., 1992; Lane, 1992). However, p53 is now known to act in many cellular processes, including cell-cycle checkpoints, DNA repair, senescence, apoptosis, angiogenesis, and the surveillance of genomic integrity (Evan and Vousden, 2001; Ko and Prives, 1996). In principle, disruption of any one or combination of these activities may explain the high frequency of *p53* mutations in human tumors (Hainaut et al., 1998). Most studies designed to identify relevant p53 tumor suppressor functions have examined the behavior of *p53* mutant tumor cells, or correlated loss of specific p53-controlled functions with tumor progression in animal models or cancer patients (Attardi and Jacks, 1999; Bardeesy et al., 1995; Kakolyris et al., 2000; Smith and Fornace, 1995). However, neither approach distinguishes between those p53 functions that are actively selected against during tumorigenesis and those that are simply consequences of p53 loss.

Attempts to directly address this issue have used mouse models to determine whether disruption of individual p53 effectors can recapitulate the effects of p53 inactivation during tumorigenesis. However, in all of these studies, the biological consequences of inactivating a specific p53 effector have not been as severe as those obtained by inactivating p53 itself. For example, inactivation of *bax*, a proapoptotic effector of p53, can accelerate tumor development in several settings, but not to the same extent as loss of p53 (Eischen et al., 2001; Yin et al., 1997). Since it is likely that p53 modulates apoptosis (and other cellular processes) through multiple effectors, it is not possible to conclude that a nonapoptotic activity of p53 contributes to tumor suppression in these settings.

We hypothesized that *complete* ablation of crucial p53 effector functions may produce tumors that are phenotypically identical to those with *p53* mutations yet retain wild-type p53. To this end, we examined the ability of dominant-acting genes that completely disable apoptosis downstream of p53 to phenocopy the effects of p53 mutations in the *Eμ-myc* transgenic mouse. These mice overexpress the *c-myc* oncogene in the B cell lineage and develop pre-B or B cell lymphoma by several months of age (Adams et al., 1985), and provide an ideal setting in which to study p53 function during tumor development. First, tumors arising in these animals closely resemble human non-Hodgkin's lymphoma (Adams et al., 1985). Second, p53 acts as a potent tumor suppressor in this model, since spontaneous *p53* mutations occur in a subset of *Eμ-myc* lymphomas (Eischen et al., 1999; Schmitt et al., 1999). Third, experimental inactivation

SIGNIFICANCE

***p53* mutations have been associated with defects in many cellular processes. In principle, the simultaneous loss of multiple p53 functions might provide an enormous advantage to *p53* mutant tumor cells. Alternatively, disruption of a single p53 activity might provide an essential capability, with the other defects arising as byproducts of p53 loss. Here we show that disruption of apoptosis is the only consequence of p53 loss required for the generation of aggressive murine lymphomas. In contrast, other p53-related defects, while present, have no further impact on tumor growth. Therefore, not all defects observed in *p53* mutant tumors contribute to the malignant phenotype. Understanding which p53 functions naturally suppress tumorigenesis in different settings should provide a framework for developing rational therapies most likely to have tumoricidal potential.**

of p53 dramatically accelerates lymphoma onset and invasiveness (Schmitt et al., 1999). Finally, as shown here, genes can be introduced into established lymphomas or premalignant hematopoietic stem cells ex vivo (Schmitt et al., 2000a), thereby making the system experimentally tractable. This latter feature allows one to study the impact of specific genes on tumor behavior following transplantation into syngeneic recipients, and to tag tumor cells with fluorescent proteins for whole body imaging of tumor behavior in live mice.

Results

To determine the contribution of apoptosis to p53-mediated tumor suppression, we utilized Bcl2 and a dominant-negative caspase 9 (Pan et al., 1998) (C9DN) as moieties that act at different levels downstream of p53 to disrupt apoptosis but not other p53 effector functions (Chiou et al., 1994; Huang et al., 1997; Soengas et al., 1999). Bcl2 or C9DN were introduced into freshly isolated *Eμ-myc* lymphoma cells (hereafter referred to as controls [ctrl.]) or *Eμ-myc p53* null lymphomas (that arose in $p53^{+/-}$ animals that invariably lose the wild-type *p53* allele (Schmitt et al., 1999), see Table 1 for genotype nomenclature of normal and lymphoma cells) using murine stem cell virus-based retroviral vectors that coexpressed Bcl2 or C9DN with green fluorescent protein (GFP) from a bicistronic message (MSCV-bcl2 and MSCV-C9DN, respectively). As a control, the same lymphomas were infected with a vector expressing GFP alone (MSCV). The infection efficiency was typically greater than 70% as assessed by flow cytometry for GFP expression (data not shown). Ctrl. lymphomas were substantially more sensitive than *p53* null lymphomas to treatment with mafosphamide (an alkylating agent) or γ-irradiation (Figure 1A; compare MSCV lanes). As predicted, both Bcl2 and C9DN markedly suppressed apoptosis in ctrl. lymphomas but did not further reduce apoptosis in *p53* null lymphomas (Figure 1A). However, consistent with their distinct modes of action, Bcl2 prevented mitochondrial cytochrome c release, whereas C9DN did not (data not shown). Together, these data imply that Bcl2 and C9DN can suppress apoptosis in lymphoma cells in a manner that is largely dependent on p53.

Next, we asked whether cells harboring apoptotic defects could be selected for during tumor expansion by using an in vivo competition assay. Mixed lymphoma populations were prepared by combining GFP-tagged ctrl.-MSCV, *p53* null-MSCV, ctrl.-bcl2, or ctrl.-C9DN lymphoma cells with non-GFP expressing ctrl. or *p53* null counterparts, such that the percentage of GFP-positive cells ranged between 4%–15% (Figure 1B, "input"). These populations were immediately injected into the tail vein of syngeneic animals, where they were allowed to expand in vivo. The peripheral lymph nodes (LN) of tumor-bearing mice were resected when they achieved a well-palpable size (>5 mm diameter) (Schmitt et al., 2000b), after which lymphoma cells were isolated and subjected to flow cytometry to determine the percentage of GFP-positive cells ("tumor," i.e., the percentage of cells expressing the transduced gene). Importantly, the percentage of ctrl.-MSCV cells mixed with uninfected ctrl. lymphomas did not change during lymphoma expansion (Figure 1B, upper left), indicating that there was no positive or negative selection against the MSCV vector [$(\%GFP_{tumor})/(\%GFP_{input}) \pm$ s.d. $= 0.93 \pm 0.27$)]. Like nullizygosity for *p53*, expression of Bcl2 or C9DN in ctrl. cells resulted in dramatic enrichment relative to unlabeled ctrl. lymphoma cells, such that virtually all of the recovered lymphoma cells were GFP-positive (Figure 1B, top panels). This effect was also p53-dependent, since *p53* null cells expressing the antiapoptotic genes showed little (Bcl2), if any (C9DN), enrichment relative to uninfected *p53* null cells (Figure 1B, bottom). These results, together with those presented in Figure 1A, indicate that Bcl2 and C9DN target apoptosis but do not affect nonapoptotic functions of p53. Hence, like p53 inactivation, disruption of apoptosis provides a potent selective advantage in vivo.

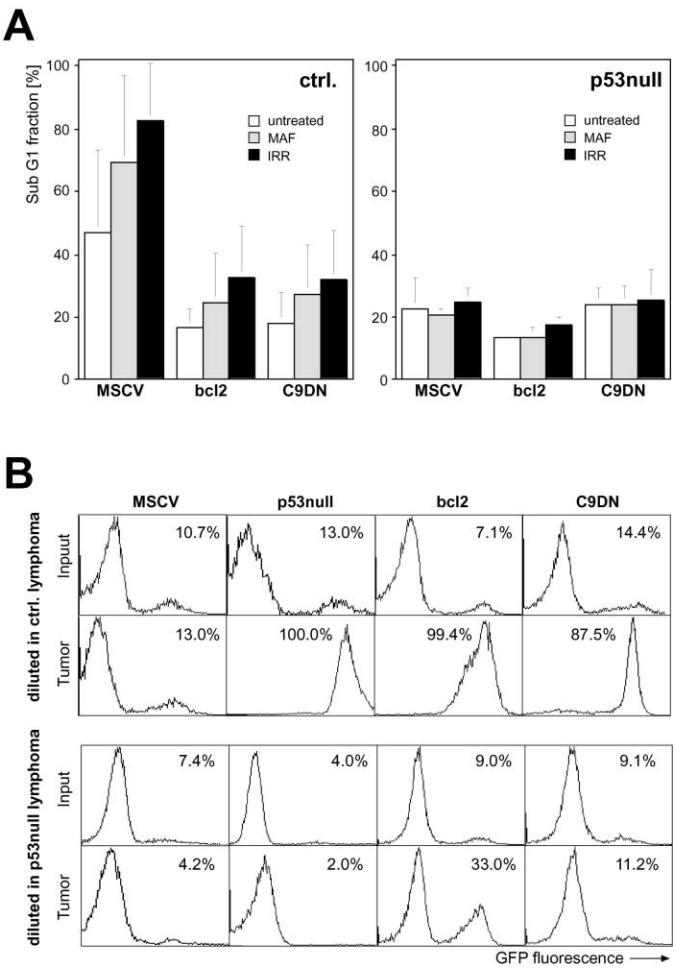

Figure 1. Enrichment for apoptotic defects during lymphoma establishment

A: Apoptosis upon exposure to DNA damaging treatments (mafosphamide, MAF, 3 μg/ml, over 6 hr, and IRR, 6 hr after 4 Gy γ-irradiation) in ctrl. (left) or *p53* null (right) lymphoma cells in vitro. Cells were transduced with an empty vector (MSCV) or retroviral constructs encoding bcl2 or a dominant-negative activity of caspase 9 (C9DN) coexpressed with GFP. Apoptotic cell death was analyzed by propidium iodide staining and flow cytometry, and was measured as fractions with less than G1 DNA content. Results shown represent the average of at least three independent experiments (± SD).

B: Lymphoma populations as in **A** (transduced with GFP-coexpressing vectors) were mixed with their corresponding untransduced primary lymphomas (see Experimental Procedures for details), adjusted to 4%–15% GFP expressing cells (exact flow cytometric values shown as "input"), and transplanted (1×10^6 cells by tail vein injection) into recipient mice. Upon tumor formation, lymph nodes were assessed for the fraction of GFP positive cells by flow cytometry ("tumor"). Shown is one representative data set out of at least two experiments each.

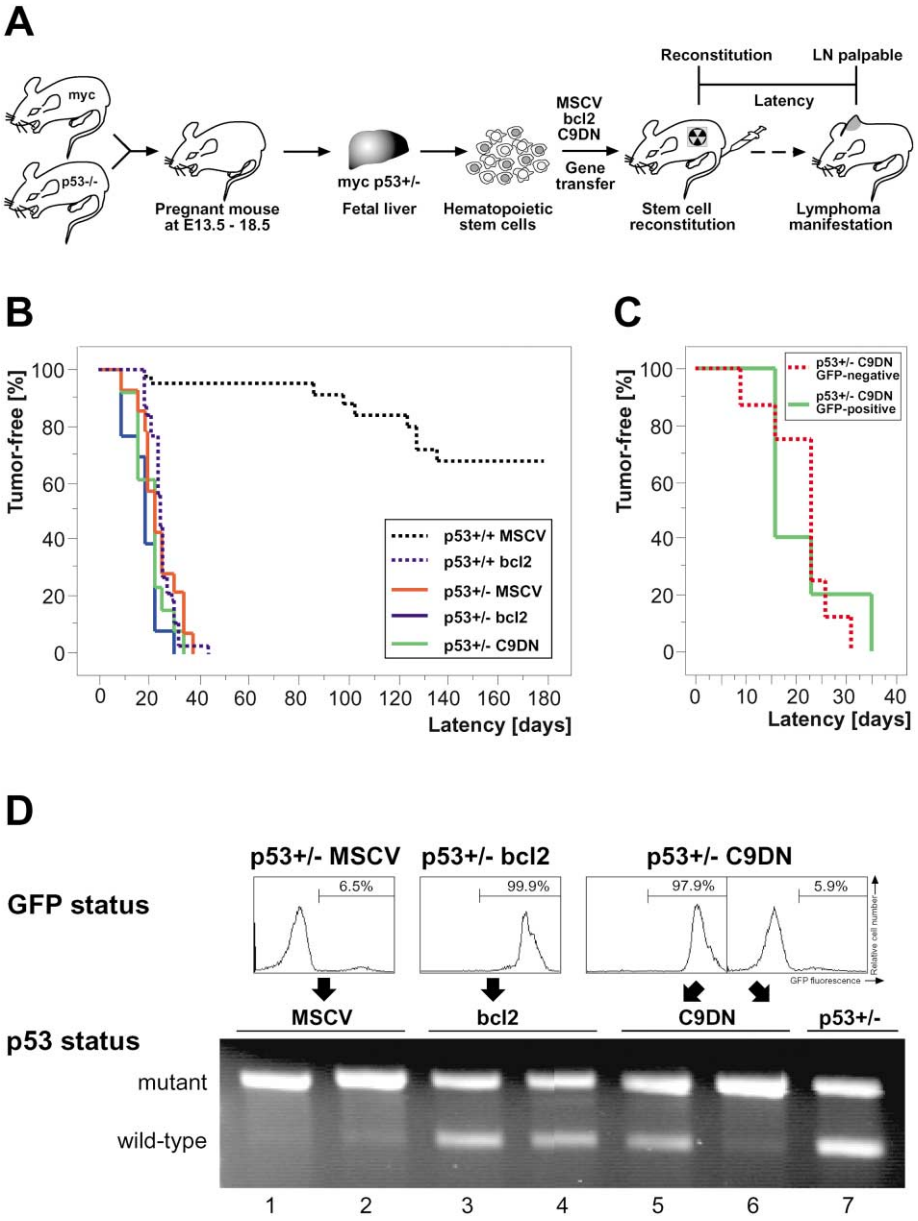

Figure 2. Genetic lesions compromising p53-mediated apoptosis protect from *p53* deletion in lymphoma development

A: *Myc*-transgenic $p53^{+/-}$ or $p53^{+/+}$ offspring were generated by crossbreeding, and fetal livers were isolated at gestational age E13.5–E18.5. Fetal liver cells transduced with MSCV, bcl2, or C9DN constructs coencoding GFP were systemically reconstituted in lethally irradiated recipients. The time between transplantation and manifestation of palpable peripheral lymph node (LN) enlargements was scored as "latency."

B: Tumor latency in recipient animals reconstituted with *myc*-transgenic $p53^{+/+}$ or $p53^{+/-}$ fetal liver cells transduced with the indicated vectors (n = 43, 38, 14, 14, 13 for $p53^{+/+}{}_{HSC}$-MSCV [hatched black line], $p53^{+/+}{}_{HSC}$-bcl2 [hatched blue line], $p53^{+/-}{}_{HSC}$-MSCV [red], $p53^{+/-}{}_{HSC}$-bcl2 [blue], and $p53^{+/-}{}_{HSC}$-C9DN [green], respectively).

C: Tumor latency in $p53^{+/-}{}_{HSC}$-C9DN derived tumors, stratified by their GFP status (GFP-negative, n = 8, hatched red line; GFP-positive, n = 5, green line). GFP status was assessed by flow cytometry at the time of tumor manifestation.

D: GFP expression status in stem cell transfer-derived lymphomas to indicate dependency of the formed tumor on the introduced transgene (top), and corresponding genomic status of the *p53* genes ($p53^{+/-}$ is included as positive control; bottom). Shown are two representative examples of each genotype.

Eμ-myc lymphomas arising in $p53^{+/-}$ mice invariably lose the wild-type *p53* allele (Hsu et al., 1995; Schmitt et al., 1999). To determine whether disruption of apoptosis downstream of p53 alleviates pressure to inactivate p53 during lymphoma development, we examined the impact of Bcl2 or C9DN expression on onset latency and *p53* status of *Eμ-myc* lymphomas arising from $p53^{+/-}$ cells. We introduced MSCV, MSCV-bcl2, or MSCV-C9DN into preneoplastic, *Eμ-myc* transgenic hematopoietic stem cells (HSC) from fetal livers of $p53^{+/-}$ mice, and propagated the transduced populations in nontransgenic, lethally irradiated recipient animals (Figure 2A). Since all animals were reconstituted with stem cells that activate *myc* during B cell development, we anticipated that most animals would develop lymphomas. This approach provides a rapid alternative to generating and crossing transgenic mice for producing complex tumor genotypes. Indeed, as has been observed in studies using germline transgenics (Strasser et al., 1990), animals reconstituted with MSCV-bcl2 transduced HSC derived from *Eμ-myc* ($p53^{+/+}$) transgenic mice developed lymphomas more rapidly than animals reconstituted with their MSCV-transduced counterparts ($P < 0.0001$; 25% tumor incidence at day 24 for MSCV-bcl2 versus day 128 for MSCV; Figure 2B).

As expected, mice reconstituted with MSCV-transduced $p53^{+/-}$ HSC developed lymphomas ($p53^{+/-}{}_{HSC}$-MSCV) extremely rapidly compared to mice receiving MSCV-transduced $p53^{+/+}$ HSC ($P < 0.0001$; Figure 2B). The percentage of GFP-positive tumors in this cohort was in the range of the infection efficiency of the fetal liver cells used to reconstitute the lethally irradiated recipients (5%–30%), again suggesting that there was no positive or negative selection for the MSCV vector. Mice reconstituted with bcl2-transduced $p53^{+/-}$ cells developed lymphomas ($p53^{+/-}{}_{HSC}$-bcl2) even more rapidly ($P < 0.0001$ versus $p53^{+/+}{}_{HSC}$-MSCV; $P = 0.03$ versus $p53^{+/-}{}_{HSC}$-MSCV; Figure 2B). In this context, 100% of the lymphomas were GFP-positive (14/14

Table 1. Designation (in bold) of lymphomas with defined genetic lesions

Normal cell genotype[a,b]	Retroviral construct	Infection of established lymphomas (lymphoma develops in the absence of the transduced gene)	Infection of hematopoietic stem cells (lymphoma develops in the presence of the transduced gene)
myc p53$^{+/+}$	no	**ctrl.**	**ctrl.**$_{HSC}$
	MSCV	**ctrl.-MSCV**	**ctrl.**$_{HSC}$**-MSCV**
	MSCV-bcl2	**ctrl.-bcl2**	**ctrl.**$_{HSC}$**-bcl2**
	MSCV-C9DN	**ctrl.-C9DN**	**ctrl.**$_{HSC}$**-C9DN**
myc p53$^{+/-}$	no	***p53*-null**	***p53*-null**$_{HSC}$
	MSCV	***p53*-null-MSCV**	***p53*-null**$_{HSC}$**-MSCV**
	MSCV-bcl2	***p53*-null-bcl2**	***p53***$^{+/-}{}_{HSC}$**-bcl2**
	MSCV-C9DN	***p53*-null-C9DN**	***p53***$^{+/-}{}_{HSC}$**-C9DN**

[a] Lymphomas arising from +/+ cells (no targeted gene deletion) form as "controls" (ctrl.).
[b] Lymphomas arising from +/− cells not preserving a functional wild-type sequence are considered "null."

cases), indicating a strong selection for the presence of Bcl2. Lymphoma onset in mice reconstituted with C9DN-transduced *p53*$^{+/-}$ HSC was similar to the *p53*$^{+/-}{}_{HSC}$-MSCV group ($P < 0.0001$ versus *p53*$^{+/+}{}_{HSC}$-MSCV), but only a subset was GFP-positive (5/13 cases). Of note, there was no difference in the tumor onset between GFP-positive versus -negative lymphomas within the *p53*$^{+/-}{}_{HSC}$-C9DN group (Figure 2C).

The expression of Bcl2 or C9DN in *Eμ-myc* lymphomas correlated precisely with the *p53* status of the lymphomas. Irrespective of their GFP status, most of the lymphomas arising from *p53*$^{+/-}$-MSCV HSC lost the wild-type *p53* allele and became *p53* null (13/14 cases; hereafter designated as *p53* null$_{HSC}$-MSCV; Figure 2D, lanes 1 and 2; see also Table 1). In contrast, virtually all of the *p53*$^{+/-}{}_{HSC}$-bcl2 lymphomas retained the wild-type *p53* allele (12/13 cases; Figure 2D, lanes 3 and 4). Remarkably, the subset of *p53*$^{+/-}{}_{HSC}$-C9DN lymphomas that was GFP-positive (and, hence, expressed C9DN; Figure 2D, lane 5) retained the wild-type *p53* allele (5/5), whereas those tumors that were GFP-negative did not (8/8; Figure 2D, lane 6). Importantly, the retention of wild-type p53 in tumors expressing Bcl2 or C9DN cannot be attributed to a cell division bias (i.e., less cell doublings required to achieve a similar tumor burden), since the wild-type *p53* allele was retained even after passaging *p53*$^{+/-}{}_{HSC}$-bcl2 and *p53*$^{+/-}{}_{HSC}$-C9DN lymphomas through syngeneic recipient mice (data not shown). Therefore, disruption of apoptosis alleviates the pressure to inactivate p53.

In addition to accelerating lymphomagenesis, p53 loss results in *Eμ-myc* lymphomas that are extremely aggressive (Schmitt et al., 1999). To determine how disruption of apoptosis downstream of p53 impacts tumor behavior, we examined the pathology of *p53*$^{+/-}$ lymphomas in which the wild-type *p53* allele was retained owing to expression of Bcl2 or C9DN. The "starry sky" morphology of cell clusters undergoing apoptosis is a hallmark of *Eμ-myc* lymphomas and related human malignancies (Adams et al., 1985; Hecht and Aster, 2000); accordingly, most ctrl.-MSCV lymphomas contained heterogeneous clusters of dying cells that were TUNEL-positive (Figure 3A). However, much like *p53* null$_{HSC}$-MSCV lymphomas, *p53*$^{+/-}{}_{HSC}$-bcl2 or *p53*$^{+/-}{}_{HSC}$-C9DN lymphomas were relatively homogeneous and contained few apoptotic cells (Figure 3A). We previously reported that *p53* null lymphomas readily invade visceral organs, whereas most control lymphomas remain restricted to the lymphoid compartment (Schmitt et al., 1999) (Figure 3B). Similarly, *p53*$^{+/-}{}_{HSC}$-bcl2 and *p53*$^{+/-}{}_{HSC}$-C9DN lymphomas grow in a highly invasive manner, for example, with pulmonary infiltration leading to destruction of the normal lung architecture (Figure 3B). Hence, disruption of apoptosis, but not primarily p53 loss, enables tumor cells to override natural growth barriers and to invade more aggressively into visceral organs outside the lymphoid compartments.

This aggressive growth pattern was further documented using whole-body fluorescence imaging, which allows visualization of GFP-tagged cells in live mice (Yang et al., 2000). Consistent with the histopathological findings, ctrl.-MSCV lymphomas were typically restricted to the LN, bone marrow, and spleen (Figure 4). In stark contrast, *p53* null$_{HSC}$-MSCV and *p53*$^{+/-}{}_{HSC}$-bcl2 lymphomas were more disseminated, apparently invading liver, kidneys, lung, and brain, despite comparable LN enlargements (Figure 4). Therefore, disruption of apoptosis downstream of p53 produces tumors that recapitulate the aggressive behavior of *p53* mutant tumors.

p53 loss is also associated with severe disturbances in several cell-cycle checkpoints and genomic integrity, leading to the hypothesis that an essential role for p53 in tumor suppression is to limit the occurrence of secondary mutations that fuel tumor progression. To evaluate the contribution of checkpoint defects to *myc*-induced lymphomagenesis, we examined the DNA damage-induced G1 and G2 checkpoints in primary cultures of *Eμ-myc* lymphomas. As predicted, *p53* null$_{HSC}$-MSCV lymphoma cells displayed profound defects in the radiation-induced G1 checkpoint, showing only a modest reduction in the S phase fraction and a G2 accumulation 20 hr after γ-irradiation (Figure 5A). Similarly, γ-irradiated *p53* null$_{HSC}$-MSCV lymphoma cells were unable to arrest properly in G2, as documented using a "mitotic trap" assay that measures the inappropriate passage of cells through G2 into mitosis in the presence of the spindle poison nocodazole (Bunz et al., 1998) (Figure 5B). Many of these inappropriately proliferating cells have a >4N DNA content, indicative of endoreduplication. (Figure 5C). Of note, some *p53* null$_{HSC}$-MSCV lymphoma cells even underwent endoreduplication in the presence of nocodazole alone, suggesting a spindle checkpoint defect (Cross et al., 1995) or a subsequent G1 arrest following adaptation to nocodazole (Lanni and Jacks, 1998). Although *p53*$^{+/-}{}_{HSC}$-bcl2 lymphomas were identical to *p53* mutant tumors with respect to accelerated tumor onset and invasiveness, they did not display the checkpoint defects associated with p53 loss. Indeed, consistent with their retention of p53, *p53*$^{+/-}{}_{HSC}$-bcl2 lymphomas preserved an intact G1 and G2 checkpoint, and did not undergo endoreduplication in the presence of spindle poisons. As expected, the p53 retained in these

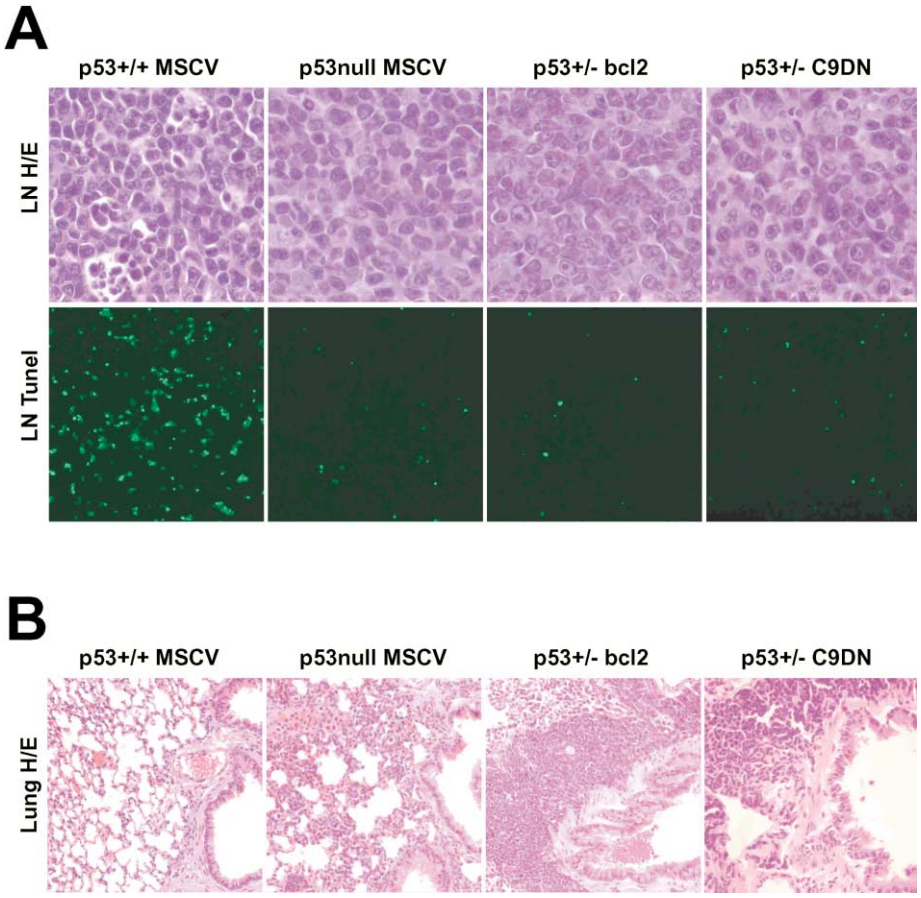

Figure 3. Apoptotic defects predispose to aggressive tumors despite retained *p53* genes

A: Hematoxilin and eosin (H/E; high power field, top) stained sections of LN of similar size. Confirmation of apoptotic cell death by the FITC-based TUNEL reaction in situ (low power field, bottom).

B: Lung tissue sections obtained from animals bearing lymphomas as in **A** showing very little pulmonary infiltration for $p53^{+/+}$-MSCV lymphoma cells (far left), but massive lung invasion by lymphomas reflecting *p53*-$null_{HSC}$-MSCV (left), $p53^{+/-}{}_{HSC}$-bcl2 (right) and $p53^{+/-}{}_{HSC}$-C9DN (far right) genetic constellations (H/E, low power field). Shown are representative examples.

tumors remained functional, since treatment with DNA damaging agents induced p53 and its transcriptional target p21 (Figure 5D).

The most common form of genomic instability that is associated with p53 loss is aneuploidy, although not all *p53* mutant tumors display this phenotype (Bunz et al., 2002; Lu et al., 2001). Indeed, freshly isolated *p53* $null_{HSC}$-MSCV lymphomas were usually aneuploid, as measured by DNA content profiles (Schmitt et al., 1999) (Figure 6, top; 4/7) and by direct counting of chromosomes in metaphase spreads (mean 48.2; range 39–107 chromosomes; $n = 5$). In contrast, $p53^{+/-}{}_{HSC}$-bcl2 and GFP-positive $p53^{+/-}{}_{HSC}$-C9DN lymphoma cells did not display aneuploidy but remained pseudodiploid with a normal chromosome count of 40 (mean 40.0 and 40.8; range 39–43 and 40–43; $n = 7$ and $n = 3$; [compared to *p53* $null_{HSC}$-MSCV] $P < 0.0001$ and $P = 0.0017$, respectively, Figure 6). Importantly, $p53^{+/-}{}_{HSC}$-C9DN lymphomas that were GFP-negative and became *p53* deficient behaved like *p53* $null_{HSC}$-MSCV cells (mean 45.8; range 39–75). Thus, apoptotic defects in the presence of intact p53 do not necessarily impose chromosomal instability. As a result, the integrity of p53-dependent cell-cycle checkpoints and chromosomal stability were uncoupled from aggressive tumor behavior and, as such, appeared to be byproducts of p53 loss.

Discussion

Given the involvement of p53 in many antiproliferative processes, it is widely assumed that the high frequency of *p53* mutations in human tumors reflects the profound advantage a developing tumor cell receives by simultaneous loss of all p53 functions (Vogelstein et al., 2000). However, in this study, we observe that this is not always the case. In fact, by introducing genes into hematopoietic stem cells of different genetic backgrounds prior to spontaneous tumor formation and by studying the resulting tumor behavior in recipient mice, we demonstrate that disruption of apoptosis downstream of p53 phenocopies p53 loss with respect to its impact on tumor onset and disseminated growth pattern. In contrast, other p53-related defects, while present, have little if any effect.

The importance of apoptosis for p53-mediated tumor suppression has been suggested from correlative studies linking p53 loss to apoptotic defects during the progression of murine and human tumors (Attardi and Jacks, 1999; Bardeesy et al., 1995), as well as by functional studies demonstrating that strictly antiapoptotic activities can accelerate tumorigenesis in transgenic mice (Eischen et al., 2001; Strasser et al., 1990; Yin et al., 1997). Furthermore, certain *p53* wild-type tumors harbor mutations that can suppress apoptosis downstream of p53 (Ionov et al., 2000; Meijerink et al., 1998; Soengas et al., 2001), and some tumor-derived *p53* mutants are defective at inducing apoptosis but not cell-cycle arrest (Aurelio et al., 2000). Nevertheless, because of the many other defects present in *p53* mutant tumor cells, it has been difficult to assess the overall contribution of apoptosis to p53-mediated tumor suppression. Here we demonstrate that inactivation of apoptosis downstream of p53 alleviates pressure to mutate *p53* during *myc*-induced lym-

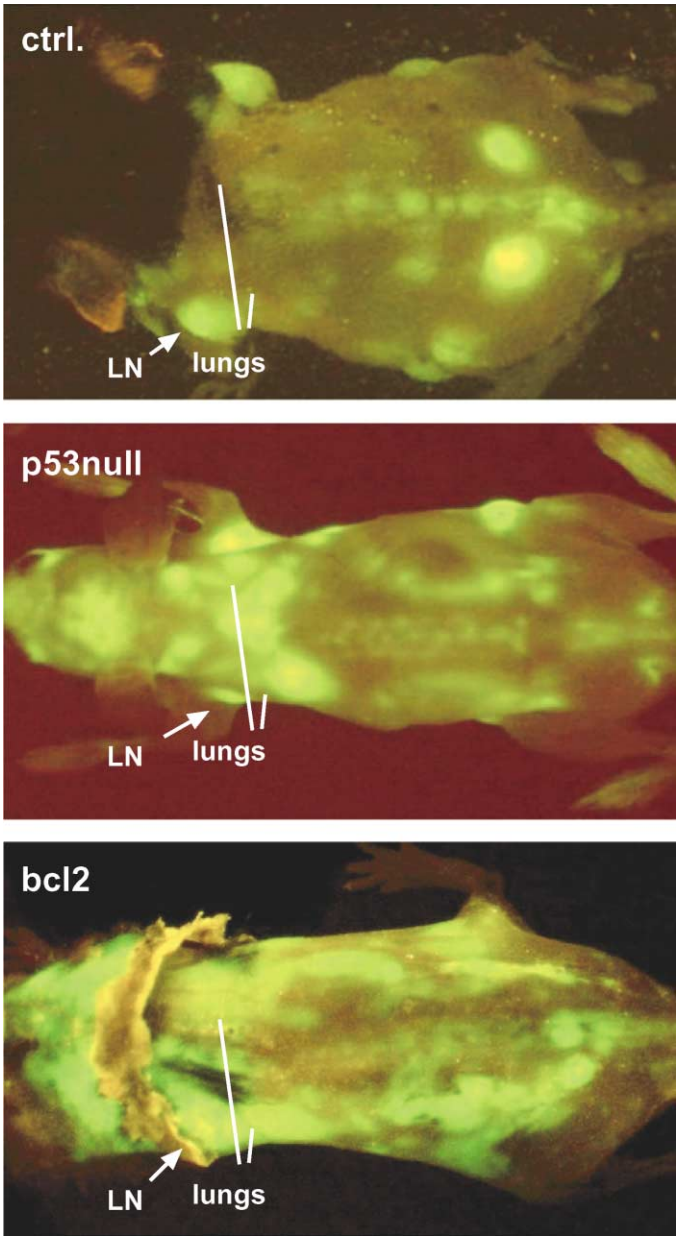

Figure 4. Whole body fluorescence imaging allows visualization of lymphoma dissemination

Lymphomas with the indicated genotypes and transduced with a GFP-coexpressing retrovirus were transplanted into recipients to monitor lymphoma dissemination in whole viable animals by GFP fluorescence. At comparable LN enlargements (e.g., axillar LN, see arrows), *p53* null and Bcl2 overexpressing lymphomas are much more disseminated, infiltrating liver, kidneys, lung (marked), and brain, while the ctrl.-MSCV lymphoma is restricted to the lymphoid compartment. GFP images are representative examples from several independent time-course experiments per genotype.

phomagenesis, implying that apoptosis is the only p53 effector function that limits tumor development in this setting. This observation is particularly interesting in light of the highly disseminated nature of *p53* mutant lymphomas, for it argues that inappropriate survival in a foreign environment—and not invasion per se—can contribute to metastatic growth.

It is noteworthy that a dominant-negative *caspase 9* allele can accelerate tumor development in the *Eμ-myc* transgenic mouse, albeit not as consistently as Bcl2. This widely used mutant allele is known to interfere with the function of the apoptosome (Fearnhead et al., 1998), which is a multiprotein complex including Apaf-1 and Caspase-9 that acts with cytochrome c released from mitochondria to promote apoptosis (Schuler and Green, 2001). Consistent with these results, *apaf-1* and *caspase 9* null fibroblasts are resistant to p53-induced apoptosis and prone to oncogenic transformation (Soengas et al., 1999). Nevertheless, it is clear that loss of caspase 9 function does not always produce a long-term survival advantage (Waterhouse et al., 2001). Moreover, while we show that C9DN can act downstream of p53 to block apoptosis, we cannot rule out the possibility that it has additional targets besides the apoptosome.

As has been observed in many settings (Eischen et al., 1999; Elson et al., 1995; Gaidano et al., 1991; Gao et al., 2000; Hsu et al., 1995; McCormack et al., 1998; Schmitt et al., 1999), p53 inactivation during *myc*-induced lymphomagenesis is associated with checkpoint defects as well as gross aneuploidy. Although it is clear that genomic instability can contribute to tumorigenesis (Honchel et al., 1995), lymphomas arising in the presence of Bcl2 or C9DN and retaining wild-type *p53* were as aggressive as those harboring *p53* mutations, but preserved key cell-cycle checkpoints and remained pseudodiploid. Therefore, the cell-cycle checkpoint defects and aneuploidy associated with *p53* mutations are byproducts of p53 loss and do not contribute to lymphomagenesis, even though they are present. This conclusion has profound implications, for it suggests that the aggressive behavior of some *p53* mutant tumors can be attributed to the immediate effects of p53 loss rather than the secondary consequences of the increased genomic instability. More importantly, our results imply that not all abnormalities observed in *p53* mutant tumors are relevant to the neoplastic phenotype.

Still, genomic instability and other byproducts of p53 loss—while not selected for initially—may confer additional capabilities to the tumor as it encounters new stresses or environments, for example, as might occur following cancer therapy or during metastatic spread. Indeed, while Bcl2 overexpression produces lymphomas that are phenotypically identical to *p53* mutant tumors, animals harboring *Eμ-myc* lymphomas overexpressing Bcl2 have a better prognosis following cancer therapy than those harboring tumors with mutant *p53* (Schmitt et al., 2002). This implies that other byproducts of p53 loss supply additional capabilities to the tumor that are revealed only under therapy. These capabilities are not conferred to *Eμ-myc* lymphomas overexpressing Bcl2. Similarly, the genomic instability that accompanies p53 inactivation confers no advantage to a transformed hamster embryo fibroblast cell line beyond that produced by disruption of apoptosis alone in a xenograft setting, but is associated with more efficient induction of experimental metastases (Gurova et al., 2002).

Our results suggest that disruption of apoptosis is sufficient to explain the occurrence of *p53* mutations in human non-Hodgkin's lymphoma, and perhaps in other cancers as well. Still, given the complexity of p53 action, it is likely that the contribution of individual effector functions to tumor suppression may vary with respect to the tissue type or inducing stimulus. For example, whereas c-Myc activates p53 to promote apoptosis,

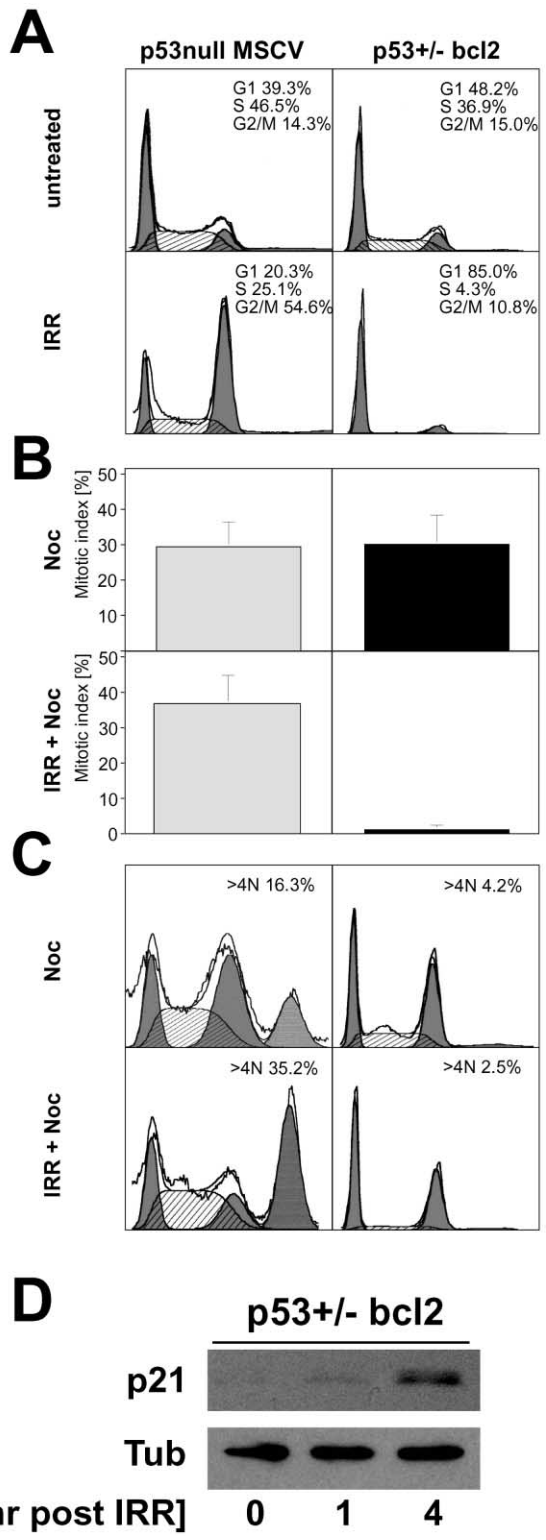

Figure 5. Aggressive growth characteristics do not require checkpoint defects

A: Cell-cycle profile analysis of freshly isolated *p53* null$_{HSC}$-MSCV and *p53*$^{+/-}{}_{HSC}$-bcl2 lymphomas untreated and 20 hr after exposure to 8 Gy γ-irradiation (note that for clarity, only pseudodiploid *p53* null$_{HSC}$-MSCV lymphomas were used in checkpoint analyses).

B: The same lymphomas were irradiated as described, but cultures were supplemented with 0.1 μg/ml of the mitotic spindle poison nocodazole 2 hr after γ-irradiation. The histograms (mean ± SD) show the fraction of cells trapped in mitosis at 20 hr after γ-irradiation (compare to untreated G2/M fraction in **A**).

C: As in **B**, but cells were subjected to DNA content analysis to assess DNA content >4N indicating endoreduplication. Data reflect experiments based on two or more preparations per genotype. Results obtained in the GFP-positive *p53*$^{+/-}{}_{HSC}$-C9DN group were similar to **A**–**C** in the *p53*$^{+/-}{}_{HSC}$-bcl2 group (data not shown).

D: Freshly isolated *p53*$^{+/-}{}_{HSC}$-bcl2 lymphomas untreated and 1 and 4 hr after exposure to 4 Gy γ-irradiation were subjected to p21 immunoblot analysis. Shown also is an α-tubulin (Tub) blot to document equal protein loading.

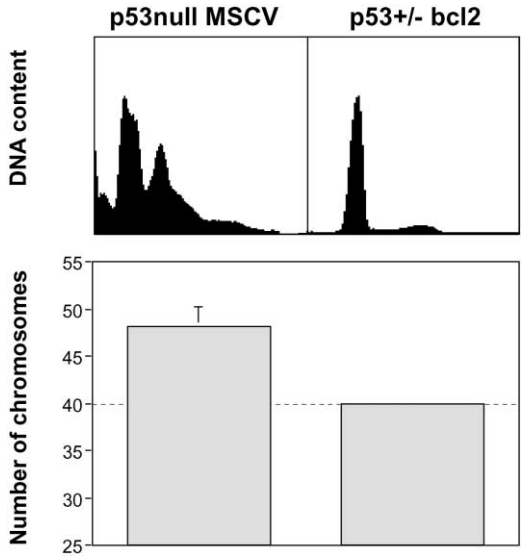

Figure 6. Aggressive lymphomas can maintain regular chromosome counts

Chromosomal instability analyzed by DNA content profiles and chromosome counts in metaphase spreads (line at 40 chromosomes indicates the regular number in mice) of (unselected) *p53* null$_{HSC}$-MSCV lymphomas and *p53*$^{+/-}{}_{HSC}$-bcl2 lymphomas (and *p53*$^{+/-}{}_{HSC}$-C9DN lymphomas, data not shown). Histograms reflect mean ± SD of at least five lymphoma populations each.

oncogenic Ras can activate p53 to induce a senescence-like arrest (Serrano et al., 1997). Hence, during *ras*-initiated tumorigenesis, disruption of senescence may provide the immediate advantage to cells acquiring *p53* mutations, whereas apoptotic defects may be byproducts of p53 loss. Defining the crucial p53 effector functions that act naturally to suppress the development of different tumor types will be important for designing targeted therapeutics that are likely to be most effective against *p53* mutant tumors.

Experimental procedures

Generation of lymphomas with defined genetic lesions

Eμ-myc transgenic mice were crossbred to *p53*$^{-/-}$ mice (both C57BL/6 inbred strains) in order to obtain *myc*-transgenic *p53*$^{+/-}$ offspring. Genotyping was performed by PCR as described (Schmitt et al., 1999). Mice were sacrificed by CO_2 euthanasia when peripheral lymph node enlargements became well-palpable, about 5 mm in the longest diameter. Lymphomas were either fixed for histopathological evaluation, or processed to single cell suspensions for subsequent assays and cell culture as described (Schmitt et al., 1999). Of note, newly cultured control lymphomas displaying reduced

spontaneous cell death by trypan blue exclusion similar to *p53* null lymphomas were excluded since they might have acquired secondary mutations in the p53 pathway (Eischen et al., 1999; Schmitt et al., 1999). Day 13.5–18.5 pregnant mice from a *myc*-transgenic to $p53^{-/-}$ cross (or to $p53^{+/-}$ for some experiments) were sacrificed to obtain fetal livers, which were minced and grown at approximately 3×10^6 cells/ml in conditions supporting hematopoietic stem cell growth (37% DMEM, 37% Iscove's modified Dulbecco's Medium [Gibco], supplemented with 20% fetal calf serum, 2% L-glutamine [200 mM], 100 U/ml penicillin/streptomycin, 5×10^{-5} M 2-mercaptoethanol, 4% 0.45 μm filtered WEHI-3B supernatant, 0.2 ng/ml recombinant murine interleukin-3, 2 ng/ml recombinant murine interleukin-6, and 20 ng/ml recombinant murine stem cell factor [all cytokines from Research Diagnostics] at 37°C in a humidified 5% CO_2 atmosphere).

A dominant-negative caspase 9 (C9DN) was generated by site-directed mutagenesis of an adenine to thymine at nucleotide position 973 of the murine cDNA resulting in a cysteine to serine exchange in the catalytic center QACGG (Pan et al., 1998). This was subcloned into MSCV-IRES-GFP (MSCV-C9DN). MSCV-bcl2-IRES-GFP (MSCV-bcl2) has been described (Schmitt et al., 2000a). Production of retroviral supernatants and transductions were carried out as previously described (Schmitt et al., 2000a); however, for infection of fetal liver cells, virions were collected in stem cell medium (see above). High-titer retroviral supernatant was passed through a 0.45 μm filter and supplemented with 4 μg/ml polybrene (Sigma). About 6×10^6 cells were infected four times by spinoculation at 600 g for 10 min in 3 ml of retroviral supernatant every 6–8 hr. 24 hr after the last infection, the fraction of GFP (green fluorescent protein) expressing cells was measured by flow cytometry (FACScalibur, Beckton Dickinson), and protein expression of the bcl2 or C9DN constructs was detected by western blot analysis using antibodies against Bcl2 (13456E, Pharmingen, 1:750 dilution) or Caspase 9 (AAP-109, Stressgen, 1:500 dilution). α-tubulin (B-5-1-2, Sigma, 1:2000 dilution) served as a loading control (Schmitt et al., 2000a) (data not shown).

For bone marrow reconstitution experiments, 6- to 8-week old C57BL/6 recipient mice received a single 10 Gy-dose of total body γ-irradiation (^{137}Cesium source; 0.8 Gy/min), and were reconstituted 6 hr later with approximately 3×10^6 viable fetal liver cells by tail vein injection. Mice were housed on autoclaved bedding in air-filtered cages and received neomycin-containing drinking water. Nonreconstituted, lethally irradiated mice were included as controls in every experiment, and typically had to be sacrificed between day 12 and 18 post irradiation due to bone marrow aplasia. Animals were euthanized upon lymphoma onset, which is defined as the occurrence of well-palpable peripheral lymph node enlargements. Statistical evaluation of tumor onset data is based on the log-rank (Mantel-Cox) test for comparison of the Kaplan-Meier event-time format, and on the unpaired t test for comparison of means and standard deviations. The genomic p53 status of $p53^{+/-}$ derived lymphoma cells was analyzed by allele specific PCR after short-term culture as described (Schmitt et al., 1999).

Whole body imaging of GFP-tagged lymphomas

Living animals underwent total body imaging of GFP-expressing lymphomas (Yang et al., 2000) at several time points after systemic transplantation of lymphoma cells transduced with a GFP-encoding retrovirus. A fluorescence stereo microscope (Leica LZ12), equipped with a 50 W mercury lamp, was used for high magnification imaging. Selective excitation of GFP was produced through a D425/60 band-pass filter and 470 DCXR dichroic mirror. Emitted fluorescence was collected through a long-pass filter GG475 (Chroma Technology) on a 3-chip cooled color CCD camera (C5810, Hamamatsu Photonics Systems). Images were taken at least in two (typically perpendicular) levels, and underwent processing for contrast and brightness with subsequent analysis by the Image Pro Plus 3.1 software (Media Cybernetics). Images of 1024×724 pixels were captured directly on a microcomputer or continuously through video output on a high resolution VCR (SLV-R1000, Sony Corp.). Imaging at lower magnification that visualized the entire animal was carried out in a light box illuminated by blue light fiber optics (Lightools Research, Inc.) and imaged using the thermoelectrically cooled color CCD camera, as described above (Yang et al., 2000).

Lymphoma establishment assays

Freshly isolated *myc*-transgenic $p53^{+/+}$ and *p53* null lymphoma cells were transduced with bcl2, C9DN, and an "empty" MSCV-IRES-GFP vector as control (MSCV) (see Table 1 for nomenclature). Upon transduction, GFP-expressing lymphomas were mixed with their corresponding untransduced counterparts (or MSCV transduced *p53* null lymphomas with untransduced ctrl. lymphomas) in order to adjust the GFP-positive fraction to 15% or less. Actual values of GFP-expressing fractions were documented by flow cytometry. Cells were transplanted as described (Schmitt et al., 2000a), and the percentage of GFP-positive lymphoma cells was assessed after tumor formation by flow cytometry.

Assessing p53 functionality and cytochrome c release

To assess p53 function, lymphomas were treated with a single dose of 4 Gy γ-irradiation and harvested 1 or 4 hr later. Lysates were subject to immunoblotting using a polyclonal antibody against p21 (C-19, Santa Cruz, 1:500 dilution) and α-tubulin as a loading control (Schmitt et al., 1999). To measure cytochrome c release, lymphoma cells expressing Bcl2 or C9DN, respectively, were left untreated or treated with either 4 Gy γ-irradiation or incubated with 10 μg/ml mafosphamide (MAF, a cyclophosphamide analog active in vitro; a gift from Asta Medica, Germany) for 6 hr, and subsequently subjected to Dounce homogenization and centrifugation to obtain a membrane fraction enriched for mitochondria. Protein extracts from equivalent cell numbers were analyzed by immunoblotting using an anti-cytochrome c antibody (556433, Pharmingen, 1:1000 dilution) for the relative amount of cytochrome c remaining in the mitochondria (Fridman et al., 2001).

Apoptosis, ploidy, and cell-cycle checkpoint assays

Cells were treated with a single dose of 4 Gy γ-irradiation or 3 μg/ml MAF and fixed in 70% ethanol after a 6 hr incubation. DNA was stained with propidium iodide, and cells were subjected to flow cytometric cell-cycle profile analysis as described (Schmitt et al., 1999). Apoptosis was assessed as the fraction with sub-G1 DNA content. Cell-cycle parameters were analyzed using the ModFit LT 2.0 software. Apoptosis of lymphoma cells in situ was visualized using a fluorescence based TUNEL (terminal deoxynucleotidyl transferase dUTP nick end labeling) assay (Roche) in accordance with the manufacturer's protocol.

Numeric karyotypic analysis was performed on DAPI stained metaphase spreads. Freshly isolated, *p53* $null_{HSC}$-MSCV, $p53^{+/-}{}_{HSC}$-bcl2 and $p53^{+/-}{}_{HSC}$-C9DN lymphoma cells were cultured in the presence of 10 μg/ml colcemide (Gibco) for 1 hr, incubated in 0.4% prewarmed KCl for 5 min at 37°C, and fixed in a 3:1 methanol/acetic acid solution. The cell suspensions were spotted onto glass slides to spread out chromosomes in metaphase. Air-dried slides were stained with DAPI (4′,6-diamidino-2-phenylindole; 1:1000 in PBS), and mounted in a DAPI-free medium (Vector). At least 50 metaphases were counted for each lymphoma preparation under a fluorescence microscope, and at least three different preparations were analyzed per genotype. The ability to arrest in G1 upon a DNA damaging insult was tested in the named genotypes 20 hr after exposure to 8 Gy γ-irradiation in vitro. Integrity of the G2 checkpoint was tested under the same conditions; however, 0.1 μg/ml of nocodazole (Fluka) was added 2 hr after γ-irradiation, thereby reproducing the mitotic trap protocol described by Bunz et al. (1998) with minor modifications. After 20 hr, aliquots of the cells were either ethanol-fixed and subjected to DNA content profiling as described above, or fixed in a solution containing 3.7% formaldehyde, 0.5% Nonidet P-40, and 10 μg/ml of the nuclear dye Hoechst 33250 in order to count the fraction of cells with mitotic morphology, i.e., nuclei with condensed, homogeneously stained chromosomes, using a fluorescence microscope. At least 200 cells were counted per lymphoma preparation, and at least three different preparations were analyzed per genotype.

Acknowledgments

We thank A. Harris and T. Jacks for mice; W.S. Pear for the WEHI-3B murine myelomonocytic leukemia cell line; G. Hannon for a murine caspase 9 construct; K. Sokol for histopathology; L. Bianco, the CSHL animal facility and C. Rosenthal for technical assistance; and G. Hannon, S. Lee, M. McCurrach, and M. Soengas for editorial advice. This work was supported by a Special Fellowship from the Leukemia & Lymphoma Society (C.A.S.), the Laurie Strauss Leukemia Foundation and a NCI postdoctoral training grant (J.S.F.), and the Rita Allen Foundation, program project grants CA13106 and CA87497 from the National Cancer Institute (S.W.L.), and 1 R43 89779 from the National Cancer Institute (R.M.H.).

Received: February 2, 2002
Revised: April 1, 2002

References

Adams, J.M., Harris, A.W., Pinkert, C.A., Corcoran, L.M., Alexander, W.S., Cory, S., Palmiter, R.D., and Brinster, R.L. (1985). The c-myc oncogene driven by immunoglobulin enhancers induces lymphoid malignancy in transgenic mice. Nature *318*, 533–538.

Attardi, L.D., and Jacks, T. (1999). The role of p53 in tumour suppression: lessons from mouse models. Cell. Mol. Life Sci. *55*, 48–63.

Aurelio, O.N., Kong, X.T., Gupta, S., and Stanbridge, E.J. (2000). p53 mutants have selective dominant-negative effects on apoptosis but not growth arrest in human cancer cell lines. Mol. Cell. Biol. *20*, 770–778.

Bardeesy, N., Beckwith, J.B., and Pelletier, J. (1995). Clonal expansion and attenuated apoptosis in Wilms' tumors are associated with p53 gene mutations. Cancer Res. *55*, 215–219.

Bunz, F., Dutriaux, A., Lengauer, C., Waldman, T., Zhou, S., Brown, J.P., Sedivy, J.M., Kinzler, K.W., and Vogelstein, B. (1998). Requirement for p53 and p21 to sustain G2 arrest after DNA damage. Science *282*, 1497–1501.

Bunz, F., Fauth, C., Speicher, M.R., Dutriaux, A., Sedivy, J.M., Kinzler, K.W., Vogelstein, B., and Lengauer, C. (2002). Targeted inactivation of p53 in human cells does not result in aneuploidy. Cancer Res. *62*, 1129–1133.

Chiou, S.K., Rao, L., and White, E. (1994). Bcl-2 blocks p53-dependent apoptosis. Mol. Cell. Biol. *14*, 2556–2563.

Cross, S.M., Sanchez, C.A., Morgan, C.A., Schimke, M.K., Ramel, S., Idzerda, R.L., Raskind, W.H., and Reid, B.J. (1995). A p53-dependent mouse spindle checkpoint. Science *267*, 1353–1356.

Eischen, C.M., Weber, J.D., Roussel, M.F., Sherr, C.J., and Cleveland, J.L. (1999). Disruption of the ARF-Mdm2-p53 tumor suppressor pathway in Myc-induced lymphomagenesis. Genes Dev. *13*, 2658–2669.

Eischen, C.M., Roussel, M.F., Korsmeyer, S.J., and Cleveland, J.L. (2001). Bax Loss impairs Myc-induced apoptosis and circumvents the selection of p53 mutations during Myc-mediated lymphomagenesis. Mol. Cell. Biol. *21*, 7653–7662.

Elson, A., Deng, C., Campos-Torres, J., Donehower, L.A., and Leder, P. (1995). The MMTV/c-myc transgene and p53 null alleles collaborate to induce T- cell lymphomas, but not mammary carcinomas in transgenic mice. Oncogene *11*, 181–190.

Evan, G.I., and Vousden, K.H. (2001). Proliferation, cell cycle and apoptosis in cancer. Nature *411*, 342–348.

Fearnhead, H.O., Rodriguez, J., Govek, E.E., Guo, W., Kobayashi, R., Hannon, G., and Lazebnik, Y. (1998). Oncogene-dependent apoptosis is mediated by caspase-9. Proc. Natl. Acad. Sci. USA *95*, 13664–13669.

Fridman, J.S., Parsels, J., Rehemtulla, A., and Maybaum, J. (2001). Cytochrome c depletion upon expression of Bcl-XS. J. Biol. Chem. *276*, 4205–4210.

Gaidano, G., Ballerini, P., Gong, J.Z., Inghirami, G., Neri, A., Newcomb, E.W., Magrath, I.T., Knowles, D.M., and Dalla-Favera, R. (1991). p53 mutations in human lymphoid malignancies: association with Burkitt lymphoma and chronic lymphocytic leukemia. Proc. Natl. Acad. Sci. USA *88*, 5413–5417.

Gao, Y., Ferguson, D.O., Xie, W., Manis, J.P., Sekiguchi, J., Frank, K.M., Chaudhuri, J., Horner, J., DePinho, R.A., and Alt, F.W. (2000). Interplay of p53 and DNA-repair protein XRCC4 in tumorigenesis, genomic stability and development. Nature *404*, 897–900.

Gurova, K.V., Kwek, S.S., Koman, I.E., Komarov, A.P., Kandel, E., Nikiforov, M.A., and Gudkov, A.V. (2002). Apoptosis inhibitor as a suppressor of tumor progression: expression of bcl-2 eliminates selective advantages for p53-deficient cells in the tumor. Cancer Biol. Ther. *1*, 39–44.

Hainaut, P., Hernandez, T., Robinson, A., Rodriguez-Tome, P., Flores, T., Hollstein, M., Harris, C.C., and Montesano, R. (1998). IARC Database of p53 gene mutations in human tumors and cell lines: updated compilation, revised formats and new visualisation tools. Nucleic Acids Res. *26*, 205–213.

Hecht, J.L., and Aster, J.C. (2000). Molecular biology of Burkitt's lymphoma. J. Clin. Oncol. *18*, 3707–3721.

Honchel, R., Halling, K.C., and Thibodeau, S.N. (1995). Genomic instability in neoplasia. Semin. Cell Biol. *6*, 45–52.

Hsu, B., Marin, M.C., el-Naggar, A.K., Stephens, L.C., Brisbay, S., and McDonnell, T.J. (1995). Evidence that c-myc mediated apoptosis does not require wild-type p53 during lymphomagenesis. Oncogene *11*, 175–179.

Huang, D.C., O'Reilly, L.A., Strasser, A., and Cory, S. (1997). The anti-apoptosis function of Bcl-2 can be genetically separated from its inhibitory effect on cell cycle entry. EMBO J. *16*, 4628–4638.

Ionov, Y., Yamamoto, H., Krajewski, S., Reed, J.C., and Perucho, M. (2000). Mutational inactivation of the proapoptotic gene BAX confers selective advantage during tumor clonal evolution. Proc. Natl. Acad. Sci. USA *97*, 10872–10877.

Kakolyris, S.A., Kaklamanis, L.G., Koukourakis, M.J., Giatromanolaki, A., Rousomoustakaki, M., Souglakos, J.C., Reppa, D.K., Georgoulias, V.A., Gatter, K.C., and Harris, A.L. (2000). Angiogenesis and p53 expression in the colorectal adenoma-carcinoma sequence. Oncol. Res. *12*, 203–208.

Kastan, M.B., Zhan, Q., El-Deiry, W.S., Carrier, F., Jacks, T., Walsh, W.V., Plunkett, B.S., Vogelstein, B., and Fornace, A.J., Jr. (1992). A mammalian cell cycle checkpoint pathway utilizing p53 and GADD45 is defective in ataxia-telangiectasia. Cell *71*, 587–597.

Ko, L.J., and Prives, C. (1996). p53: puzzle and paradigm. Genes Dev. *10*, 1054–1072.

Lane, D.P. (1992). Cancer. p53, guardian of the genome. Nature *358*, 15–16.

Lanni, J.S., and Jacks, T. (1998). Characterization of the p53-dependent postmitotic checkpoint following spindle disruption. Mol. Cell. Biol. *18*, 1055–1064.

Lu, X., Magrane, G., Yin, C., Louis, D.N., Gray, J., and Van Dyke, T. (2001). Selective inactivation of p53 facilitates mouse epithelial tumor progression without chromosomal instability. Mol. Cell. Biol. *21*, 6017–6030.

McCormack, S.J., Weaver, Z., Deming, S., Natarajan, G., Torri, J., Johnson, M.D., Liyanage, M., Ried, T., and Dickson, R.B. (1998). Myc/p53 interactions in transgenic mouse mammary development, tumorigenesis and chromosomal instability. Oncogene *16*, 2755–2766.

Meijerink, J.P., Mensink, E.J., Wang, K., Sedlak, T.W., Sloetjes, A.W., de Witte, T., Waksman, G., and Korsmeyer, S.J. (1998). Hematopoietic malignancies demonstrate loss-of-function mutations of BAX. Blood *91*, 2991–2997.

Pan, G., O'Rourke, K., and Dixit, V.M. (1998). Caspase-9, Bcl-XL, and Apaf-1 form a ternary complex. J. Biol. Chem. *273*, 5841–5845.

Schmitt, C.A., McCurrach, M.E., de Stanchina, E., Wallace-Brodeur, R.R., and Lowe, S.W. (1999). INK4a/ARF mutations accelerate lymphomagenesis and promote chemoresistance by disabling p53. Genes Dev. *13*, 2670–2677.

Schmitt, C.A., Rosenthal, C.T., and Lowe, S.W. (2000a). Genetic analysis of chemoresistance in primary murine lymphomas. Nat. Med. *6*, 1029–1035.

Schmitt, C.A., Wallace-Brodeur, R.R., Rosenthal, C.T., McCurrach, M.E., and Lowe, S.W. (2000b). DNA damage responses and chemosensitivity in the Eμ-myc mouse lymphoma model. Cold Spring Harb. Symp. Quant. Biol. *LXV*, 499–510.

Schmitt, C.A., Fridman, J.S., Yang, M., Lee, S., Baranov, E., Hoffman, R.M., and Lowe, S.W. (2002). A senescence program controlled by p53 and $p16^{INK4a}$ contributes to the outcome of cancer therapy. Cell, in press.

Schuler, M., and Green, D.R. (2001). Mechanisms of p53-dependent apoptosis. Biochem. Soc. Trans. *29*, 684–688.

Serrano, M., Lin, A.W., McCurrach, M.E., Beach, D., and Lowe, S.W. (1997). Oncogenic ras provokes premature cell senescence associated with accumulation of p53 and $p16^{INK4a}$. Cell *88*, 593–602.

Smith, M.L., and Fornace, A.J., Jr. (1995). Genomic instability and the role of p53 mutations in cancer cells. Curr. Opin. Oncol. *7*, 69–75.

Soengas, M.S., Alarcon, R.M., Yoshida, H., Giaccia, A.J., Hakem, R., Mak, T.W., and Lowe, S.W. (1999). Apaf-1 and caspase-9 in p53-dependent apoptosis and tumor inhibition. Science *284*, 156–159.

Soengas, M.S., Capodieci, P., Polsky, D., Mora, J., Esteller, M., Opitz-Araya, X., McCombie, R., Herman, J.G., Gerald, W.L., Lazebnik, Y.A., et al. (2001). Inactivation of the apoptosis effector Apaf-1 in malignant melanoma. Nature *409*, 207–211.

Strasser, A., Harris, A.W., Bath, M.L., and Cory, S. (1990). Novel primitive lymphoid tumours induced in transgenic mice by cooperation between myc and bcl-2. Nature *348*, 331–333.

Vogelstein, B., Lane, D., and Levine, A.J. (2000). Surfing the p53 network. Nature *408*, 307–310.

Waterhouse, N.J., Goldstein, J.C., von Ahsen, O., Schuler, M., Newmeyer, D.D., and Green, D.R. (2001). Cytochrome c maintains mitochondrial transmembrane potential and ATP generation after outer mitochondrial membrane permeabilization during the apoptotic process. J. Cell Biol. *153*, 319–328.

Yang, M., Baranov, E., Jiang, P., Sun, F.X., Li, X.M., Li, L., Hasegawa, S., Bouvet, M., Al-Tuwaijri, M., Chishima, T., et al. (2000). Whole-body optical imaging of green fluorescent protein-expressing tumors and metastases. Proc. Natl. Acad. Sci. USA *97*, 1206–1211.

Yin, C., Knudson, C.M., Korsmeyer, S.J., and Van Dyke, T. (1997). Bax suppresses tumorigenesis and stimulates apoptosis in vivo. Nature *385*, 637–640.